Progress In Electromagnetics Research B, Vol. 37, 59–80, 2012

ACCURATE AND EFFICIENT ANALYSIS OF PLANAR ELECTROMAGNETIC BAND-GAP STRUCTURES FOR POWER BUS NOISE MITIGATION IN THE GHZ BAND

F. de Paulis* **and A. Orlandi**

UAq EMC Laboratory, University of L'Aquila, L'Aquila, Italy

Abstract—Noise reduction in PCB is a major concern in the present digital electronic systems with data rate beyond 10 Gbps. The noise, due to simultaneous switching noise, radiation from signal vias crossing the planes, etc. can propagate within parallel plane cavity at its resonant frequencies, thus allowing coupling between integrated circuits (ICs) far from each other. Electromagnetic band-gap (EBG) structures are largely employed as noise reduction technique. This paper presents a quick and efficient analytical approach for evaluating the EBG noise reduction performances in terms of band-gap limits. The study is based on the physics behavior of the planar EBG structures, focusing on its resonant properties. The resonant modes of the EBG cavity are affected by the additional inductance of the patterned plane respect to the case of the ideal solid plane cavity. The formulas provided, based on the quantification of such inductance, can be easily implemented and employed for a quick layout design of power planes in multilayer PCBs, as shown in a practical example of a partial EBG plane.

1. INTRODUCTION

Nowadays, the ever growing data rate required by modern digital electronic systems increases the importance of noise mitigation. The integration of multiple functionalities within the same printed circuit board (PCB) and package also requires high level of noise isolation. High speed switches in digital systems generate the well-known simultaneous switching noise (SSN) that can propagate across the PCB through the cavities made by power planes [1]. Discontinuities along the high speed interconnects, such as vias and imbalances in differential

Received 4 October 2011, Accepted 30 November 2011, Scheduled 7 December 2011

* Corresponding author: Francesco De Paulis (francesco.depaulis@univaq.it).

traces are also a source of noise [2–7]. Mixed signal systems require isolation of the analog circuitry from the digital section to decouple the current return paths, avoiding spurious signals to affect the RF functionalities [8, 9]. Electromagnetic Band-Gap (EBG) structures have been introduced firstly for isolating adjacent antennas [10–15]. Later they start to be considered as a simple and easy-to-design approach to be implemented in PCBs for SSN rejection in the GHz range, where usual techniques for power bus decoupling, i.e., bypass capacitors, are not effective [16]. Many contributions have been proposed for designing EBG geometries to reduce noise propagation within the power planes in PCB and packages [17–21]. They have been studied also as a simple way to reduce the common mode noise current and thus unwanted radiation from PCBs [22–25].

The planar EBG is made by a sequence of patches connected by narrow bridges, thus altering the ideal solid plane pair geometry usually employed for power delivery purposes and signal/power return. The patterned plane, together with an adjacent solid plane, builds a cavity with a frequency response characterized by a band-gap.

Several methods have been proposed, [26–30] based on equivalent circuit models and the dispersion diagram for analyzing the behavior of the EBG structures. This paper extends the idea of associating an inductance to the patterned plane, as sum of the patch and bridge inductances; thus achieving a larger total inductance than the solid plane case [31]. This inductance is responsible for altering the regular resonant behavior of the cavity modes, and for generating the band-gap. The concept of the excess of inductance associated with the patterned EBG plane is applied in this work. The procedure for accurately and easily analyzing the electromagnetic behavior of an EBG cavity, focusing on the identification of the band-gap lower and upper limits, f_{Low} and f_{High}, respectively, is developed. The relationships between the f_{High} and the bridge length is offered studying the impact of the bridge on the electromagnetic behavior of the patch at its resonant frequency. The effect of the number of patches on the f_{Low} is also investigated, and analytical expressions that describe the f_{Low} asymptotic behavior for an increasing number of patches are derived. The analytical results are validated through several numerical simulations in Sections 2, 3, and 5, whereas Section 4 validates the proposed approach through experimental results. The present procedure can be quickly implemented and employed at an early design stage of the PCB layout for minimizing the effects of the SSN and noise propagation within the power/ground planes. An example of a practical application of such planar EBG on a typical PCB geometry is also provided.

2. ANALYSIS OF PLANAR EBG

2.1. Fundamental Behavior of Planar EBG

The planar EBG structure alters the typical geometry of two adjacent solid planes that are commonly used as a power delivery network in multilayer PCB. The resonant behavior of a cavity made by two adjacent solid power planes is modeled as a cavity having Perfect Electric Conductor (PEC) boundary conditions at the top and bottom walls (power planes), and Perfect Magnetic Conductor (PMC) boundary conditions at the side walls [3, 4]. The typical dimensions in multilayer PCB such as the thin dielectric between the two planes ($d \ll A$, $d \ll B$, $d \ll \lambda$, where λ is the wavelength associated with the frequency of interest) are of the order of few mils. This leads to simplify the solution of the Helmoltz equations, and thus the dispersion relation, leading to the expression in (1) [32] for the frequencies associated with the resonant TM modes inside the cavity:

$$f_{TMz,mn} = \frac{c}{2\pi\sqrt{\varepsilon_r}}\sqrt{\left(\frac{m\pi}{A}\right)^2 + \left(\frac{n\pi}{B}\right)^2} \tag{1}$$

where A and B are the dimensions of the cavity along the x and y dimensions, ε_r is the electric permittivity of the dielectric, and c is the speed of light. The modes are identified as TMz since the thin cavity leads to constant electric and magnetic fields along the z direction. The typical behavior of a cavity is given in Figure 1 (solid curve). The model has the following dimensions, $A = 5\,\text{mm}$, $B = 17\,\text{mm}$, dielectric thickness $d = 0.4\,\text{mm}$, $\varepsilon_r = 4.4$. The three dimensional (3D) electromagnetic (EM) solver CST MicroWave Studio [33] is employed for simulating the model, as well as for the numerical calculations in Sections 2, 3, and 5. The simulation ports for computing the insertion loss $|S_{21}|$ are located at $x = 2\,\text{mm}$, $y = 2\,\text{mm}$ (Port 1), and at $x = 3\,\text{mm}$, $y = 15\,\text{mm}$ (Port 2). The port are defined as vertical excitations from the bottom PEC wall to the top PEC wall. Figure 1 shows the first five resonant mode frequencies calculated using (1), perfectly corresponding to the peaks in the $|S_{21}|$ curve. The resonant behavior of the mentioned ideal cavity can be modified if one of the two planes is etched accordingly, obtaining a sequence of square patches connected by narrow bridges, as in Figure 2. The electromagnetic field inside the cavity, at the resonant frequencies, is affected by the altered geometry since the conduction current is forced to flow through the narrow bridges. This effect impacts the resonant frequencies that are shifted down, as we can see from the results in Figure 1, dashed curve. The etched plane in Figure 2 is made by $N = 3$ square patches along the y direction.

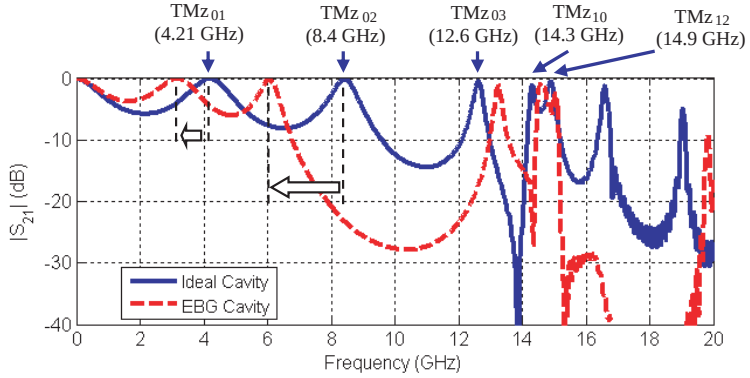

Figure 1. Simulated $|S_{21}|$ of the solid plane cavity and of the EBG cavity in Figure 2.

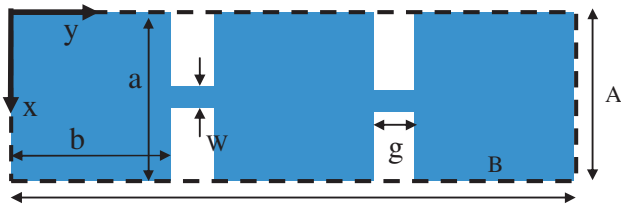

Figure 2. Etched top plane made by $N = 3$ square patches ($a = b = 5\,\text{mm}$) connected by two narrow bridges ($w = 0.5\,\text{mm}$, $g = 1\,\text{mm}$) with outline as the solid plane cavity with $A = 5\,\text{mm}$, $B = 17\,\text{mm}$.

A circuit interpretation of this behavior can be given introducing the concept of additional inductance associated with the bridges, compared to the inductance of the solid cavity [31]. The shift impacts only some of the resonant modes, up to the mode $\text{TMz}_{0,N-1}$, where N is the number of patches along the y direction. Beyond this point, there is the mode with index equal to N. This mode can be associated either to the whole patterned cavity, or as the first resonance of the single patch cavity (the small cavity made by each square patch and the solid plane underneath). The mode $\text{TMz}_{0,N}$ of the whole cavity corresponds qualitatively to the mode TMz_{10} (TMz_{01}) of the single patch cavity, that occurs always at the same frequency, and it is not affected by the shift. Therefore a band-gap is generated between the $\text{TMz}_{0,N-1}$ mode of the whole EBG cavity and the first resonance mode (TMz_{10}) of the single patch cavity. The mode $\text{TMz}_{0,N-1}$ of the EBG cavity identifies the lower limit of the band-gap, f_{Low}, and the first resonant mode of the single patch identifies the upper limit of the band-gap,

f_{High}. The accurate quantification of these limits represents the key point for efficiently designing the EBG structure.

2.2. Identification of The Band-gap Limits: $\mathbf{F_{High}}$

The upper limit of the band-gap, f_{High}, is associated with the first resonant mode (TMz_{10}) of the single patch cavity [31]. It can be easily identified by substituting the proper parameters into (1), obtaining (2).

$$f_{\text{High}} = f_{TMz,10} = \frac{c}{2a\sqrt{\varepsilon_r}} \tag{2}$$

where a is the size of the square patch. Equation (2) is a good approximation for the identification of the band-gap upper limit, even though it does not describe exactly the EM behavior of the EBG structure. An advanced study is carried out herein for a more precise identification of f_{High}.

The investigation of the first resonance after the band-gap leads to take into account the bridge length and its impact on the f_{High}. Some additional models are simulated based on the $1 \times N$ array of patches, with $N = 5$. The patch size is the same as from Figure 2 ($a = b = 5\,\text{mm}$), whereas the bridge dimensions w and g are varied for a parametric analysis. Figure 3 shows the simulation results of four models varying the bridge length g, and keeping its width constant $w = 0.5\,\text{mm}$. The f_{High} value from (2) is 14.3 GHz; however the first resonance after the band-gap is at lower frequency; it is smaller for longer bridges. Figure 4 reports the pattern of the simulated electric field $|E_z|$at the resonances occurring at 13.4 GHz, 13 GHz, 12.3 GHz, and 11.8 GHz for the cases with $g = 0.5\,\text{mm}$, $g = 1\,\text{mm}$, $g = 2\,\text{mm}$, $g = 3\,\text{mm}$, respectively. The pattern is very similar for the four figures,

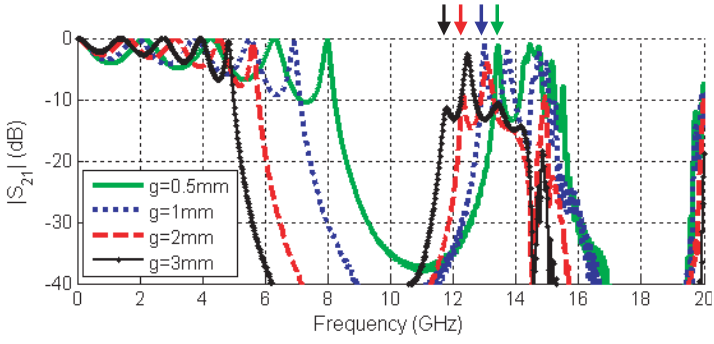

Figure 3. $|S_{21}|$ of the 5×1 patch array with $a = b = 5\,\text{mm}$, $w = 0.5\,\text{mm}$, $g = 0.5,\ 1, 2, 3\,\text{mm}$.

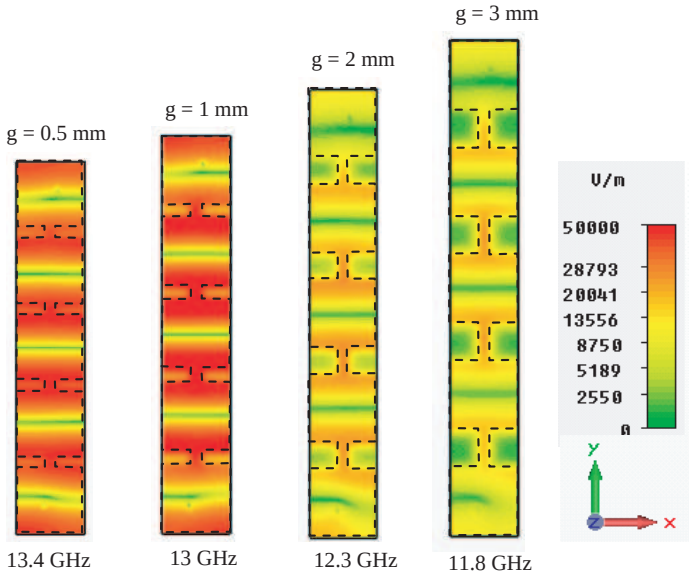

Figure 4. $|E_z|$ pattern at the first resonance after the band-gap, occurring at 13.4 GHz, 13 GHz, 12.3 GHz, and 11.8 GHz for the cases with $g = 0.5$ mm, $g = 1$ mm, $g = 2$ mm, $g = 3$ mm, respectively.

beside the E-field amplitude that increases for shorter bridge models. The quantification of the frequency difference is offered in Figure 5 which summarizes the resonance values and the percentage difference from the ideal 14.3 GHz value.

The difference in frequency value can be kept within a certain limit (i.e., below 10 %) by designing a bridge smaller than the 20 % of the patch size. It is worth noticing that the longer bridge also affects the f_{Low}. This behavior, as mentioned before, can be addressed to the larger inductance associated with the longer bridge, that shift down the first $N - 1$ modes.

An additional simulation is carried out keeping the bridge length constant, $g = 1$ mm, and varying the bridge width $w = 0.2$, 0.5, and 1 mm. The results are shown in Figure 6. The bridge width does not impact the f_{High} since all the three models provide an f_{High} around 13 GHz. The inductance associated with the three bridges increases for narrower bridges, thus leading to larger shift toward lower frequency of the first $N - 1$ resonant modes. An accurate design of an EBG in terms of band-gap upper limit can be done referring to (2), trying to keep the bridge length as small as possible, and keeping the f_{High} closer to the TMz_{10} mode of the single patch cavity.

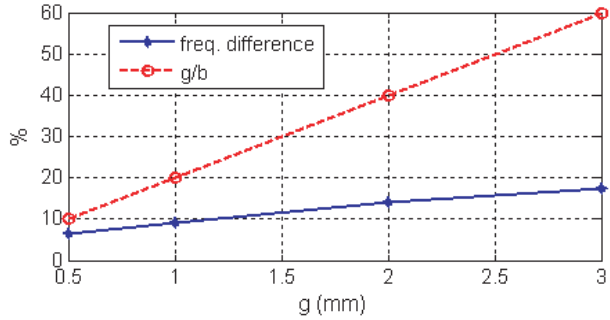

Figure 5. Evaluation of the percentage difference between the ideal TMz_{10} resonant frequency 14.3 GHz of the single patch cavity, and the first resonance after the band-gap for the four considered models (solid curve). Percentage ratio between the bridge length g and the patch size b (dashed curve).

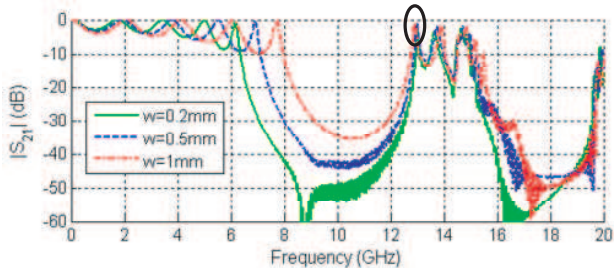

Figure 6. $|S_{21}|$ of the 1×5 patch array with $a = b = 5$ mm, $g = 1$ mm, $w = 0.2, 0.5, 1$ mm.

2.3. Identification of The Band-gap Limits: F_{Low}

The calculation of the lower limit of the band-gap, f_{Low}, is more difficult and requires a deeper study. However, based on the concept of the excess of inductance associated with the narrow bridges, in [31] the value of f_{Low} has been quantified through an expression similar to (2).

The main ideas in [31] are briefly recalled for clarity. The concept of the bridge inductance contributes to increase the overall cavity inductance; some results are provided in [31] varying the bridge width, demonstrating that a larger bridge has associated a lower inductance value, thus achieving smaller frequency shift of the first $N-1$ resonant modes. The concept that only the first $N-1$ resonant modes are shifted down is confirmed by the results shown previously, i.e., in Figure 1,

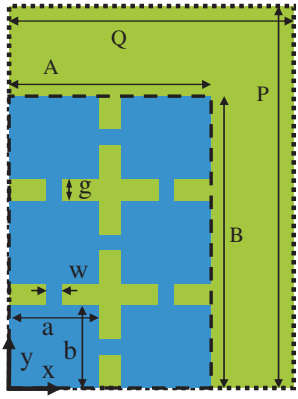

Figure 7. Top view of the model for the 2×3 EBG matrix (blue color) with $a = b = 5\,\text{mm}$, $g = 1\,\text{mm}$, $w = 0.5\,\text{mm}$, Port 1 at (2 mm, 2 mm), Port 2 at (9 mm, 15 mm). Its equivalent solid plane counterpart (green color), Port 1 at (2 mm, 2 mm), Port 2 at (11.8 mm, 20.6 mm).

where the first 2 modes of the 1×3 EBG geometry are moved from 4.21 GHz to 3.2 GHz (TMz_{01}) and from 8.4 GHz to 6.1 GHz (TMz_{02}), leaving a band-gap from 6.1 GHz to 13.2 GHz. Similar trend is found looking at the results in Figure 3 and Figure 6. The band-gap for the 1×5 EBG case is related to the shift of the first 4 modes. This concept can be extended when considering a two dimensional (2D) geometry, i.e., an $M \times N$ matrix of patches. The modes that will be affected by the shift toward lower frequency are those with index less than M and N. therefore the last mode before the band-gap can be identified as the $\text{TMz}_{M-1,N-1}$. A simple model made by a 2×3 patches is simulated and it is shown in Figure 7. The $|S_{21}|$simulation results are provided in Figure 8, (dashed curve). The geometry is based on the patch and bridge dimensions given in Figure 2, with $a = b = 5\,\text{mm}$, $g = 1\,\text{mm}$, and $w = 0.5\,\text{mm}$. The stack-up parameters are the dielectric thickness $d = 0.4\,\text{mm}$, metal thickness $t = 0.017\,\text{mm}$, and dielectric permittivity $\varepsilon_r = 4.4$.

The first resonant modes that are shifted, up to the $\text{TMz}_{M-1,\,N-1}$ mode, could be considered as associated with a solid plane cavity with dimensions larger that the overall size of the patterned cavity, such as length $P > B$, and $Q > A$. If the P and Q values can be determined, then the f_{Low} can be seen as the mode $\text{T}_{M-1,\,N-1}$ of the equivalent enlarged geometry, as in (3).

$$f_{TMz,\,M-1,\,N-1} = \frac{c}{2\sqrt{\varepsilon_r}} \sqrt{\left(\frac{M-1}{Q}\right)^2 + \left(\frac{N-1}{P}\right)^2} \tag{3}$$

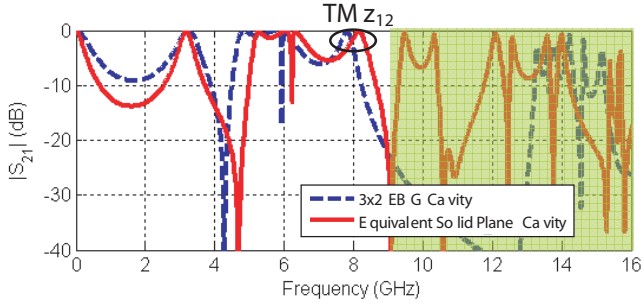

Figure 8. $|S_{21}|$ of the 2×3 EBG matrix with $a = b = 5\,\text{mm}$, $g = 1\,\text{mm}$, $w = 0.5\,\text{mm}$.

The idea of the equivalent enlarged cavity based on the concept of equivalent total inductance is described analytically in (4), assuming one dimensional (1D) array of patches both along the x and y directions [31]. The total inductance along each direction is computed as sum of the inductances of the M (N) patches and the $M-1$ ($N-1$) bridges. Then it is set equal to the inductance of a parallel plane transmission line (PPTL) of length Q (P) and width b (a), as defined in (5).

$$L_{tot,\,X} = \mu_0 d\frac{Q}{b} = ML_{patch,\,X} + (M-1)\,L_{bridge} \tag{4a}$$

$$L_{tot,\,Y} = \mu_0 d\frac{P}{a} = NL_{patch,\,Y} + (N-1)\,L_{bridge} \tag{4b}$$

$$L_{\text{PPTL}} = \mu_0 d\frac{\text{Length}_{\text{PPTL}}}{\text{Width}_{\text{PPTL}}} \tag{5}$$

$$L_{\text{PPTL}} = \mu_0 d \tag{6}$$

where d is the dielectric thickness. Equation (5) is also employed for calculating the L_{patch} in (4); for square patches, thus for a patch having equal values of length and width, (5) reduces simply to (6). The dimensions P and Q of the equivalent solid plane cavity can be easily derived from (4), as in (7). The bridge can be approximated as microstrip kind transmission line [32], whose inductance can be computed as in (8).

$$Q = \frac{b}{\mu_0 d}\left(NL_{patch,X} + (N-1)\,L_{bridge}\right) \tag{7a}$$

$$P = \frac{a}{\mu_0 d}\left(ML_{patch,Y} + (M-1)\,L_{bridge}\right) \tag{7b}$$

$$L_{bridge} = \begin{cases} l \cdot \frac{60}{c_0} \ln\left(\frac{8d}{w} + \frac{w}{4d}\right) & \frac{w}{d} \leq 1 \\ l \cdot \frac{120\pi}{c_0} \left[\frac{w}{d} + 1.393 + 0.667 \ln\left(\frac{w}{d} + 1.444\right)\right]^{-1} & \frac{w}{d} \geq 1 \end{cases} \tag{8}$$

The lower limit of the band-gap, $f_{\text{Low}} = f_{TMz,\,M-1,\,N-1}$, can be computed as in (3) by using (7). This procedure is applied to the 2×3 EBG structure in Figure 7 obtaining the equivalent inductances $L_{tot,X} = 1.38\,\text{nH}$ and $L_{tot,Y} = 2.27\,\text{nH}$. The following equivalent solid plane dimensions $P = 13.8\,\text{mm}$ and $Q = 22.6\,\text{mm}$ are obtained applying (7). The equivalent geometry is simulated obtaining the solid curve in Figure 8. The first modes, up to the one with index $m = M - 1 = 1$ and $n = N - 1 = 2$ occurs at frequencies close to those of the patterned 3×2 EBG cavity. The percentage error between each one of the first five modes are: 2.1% (TMz_{01}), 8.9% (TMz_{10}), 4.5% (TMz_{11}), 5.7% (TMz_{02}), 4.6% (TMz_{12}). The error is always below 10%; the mode TMz_{12}, related to the identification of f_{Low}, has an error less than 5%.

3. CHARACTERIZATION OF F_{LOW} FOR DIFFERENT PATCH MATRIX CONFIGURATION

A complete analysis is carried out in this sub-section studying f_{Low} for several patch configurations. The simplest geometry is the 1D sequence of patches, thus achieving a $M \times 1$ ($1 \times N$) array. However, a more general EBG configuration is based on the 2D patch matrix, as the 2×3 EBG structure in Figure 7. The aim of this section is to completely characterize the EBG for geometries made by a large number of patches, theoretically for M, $N \to \infty$.

3.1. $M \times 1$ Array of Patches

This section studies the geometry based on the $M \times 1$ array of patches. Equation (3) can be combined with (7a) to obtain (9), and then the limit for $M \to \infty$ can be evaluated as in (10):

$$f_{\text{Low}} = f_{TM_{M-1,0}} = \frac{c_0}{2\sqrt{\varepsilon_r}} \frac{M-1}{Q} = \frac{c_0}{2\sqrt{\varepsilon_r}} \frac{M-1}{M \cdot L_{patch} + (M-1) \cdot L_{bridge}} \frac{\mu_0 d}{b} \tag{9}$$

$$f_{\text{Limit}} \lim_{M \to \infty} f_{\text{Low}} = \frac{c_0 \mu_0 d}{2b\sqrt{\varepsilon_r}} \lim_{M \to \infty} \frac{M-1}{M \cdot L_{patch} + (M-1) \cdot L_{bridge}} = \frac{c_0 \mu_0 d}{2b\sqrt{\varepsilon_r}} \frac{1}{L_{patch} + L_{bridge}} \tag{10}$$

The f_{Limit} in (10) represents the upper limit for f_{Low} for an increasing number of patches. The ratio between (9) and (10) can be evaluated obtaining a normalized frequency, as in (11).

$$f_{Norm}\frac{f_{\text{Low}}}{f_{\text{Limit}}} = \frac{(M-1)(L_{patch}+L_{bridge})}{M\cdot L_{patch}+(M-1)\cdot L_{bridge}} = \frac{(M-1)(L_{patch}+L_{bridge})}{(M-1)(L_{patch}+L_{bridge})+L_{patch}} \tag{11}$$

Some test cases are simulated based on a model similar to the one given in Figure 2, maintaining the same bridge size ($w = 0.5$ mm, $g = 1$ mm) and stack-up properties ($\varepsilon_r = 4.4$, $d = 0.4$ mm). The patch size is varied as follows, $a = b = 5$, 10, 20 mm. The number of patches M goes from 2 to 100 in (9) and (10); the simulation results are shown in Figure 9. The results of the 3D simulations varying M from 2 to 20 are shown in Figure 10. The f_{Low} increases for larger values of M, as clearly visible in Figures 9 and 10. The f_{Limit} in (11) is computed using the f_{Low} from (9) and the $f_{\text{Low\_Sim}}$ extracted from the 3D simulation results given in Figure 10 (the identification of f_{Low} for the $b = 5$ mm looking at the $|S_{21}|$ is difficult for $M > 15$ due to its very low amplitude). The results are shown in Figure 11. The difference between the analytical quantification of f_{Low} and the value extracted from the simulated data is computed using (12). The results are shown in Figure 12. The error decreases as the number of patches increases, up to $M = 6$–8 patches. Beyond this value the identification of the last resonant mode $\text{TMz}_{M-1,0}$ from the data in Figure 10 is difficult since peak amplitude decreases getting close to the band-gap lowest amplitude. The error is below 20 % for $M > 4$

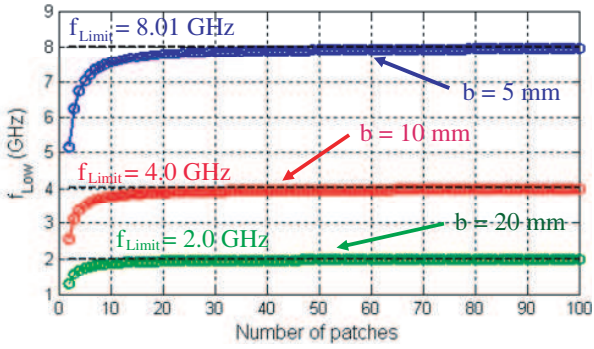

Figure 9. Analytical evaluation of f_{Low} for different patch size ($b = 5$, 10, 20 mm).

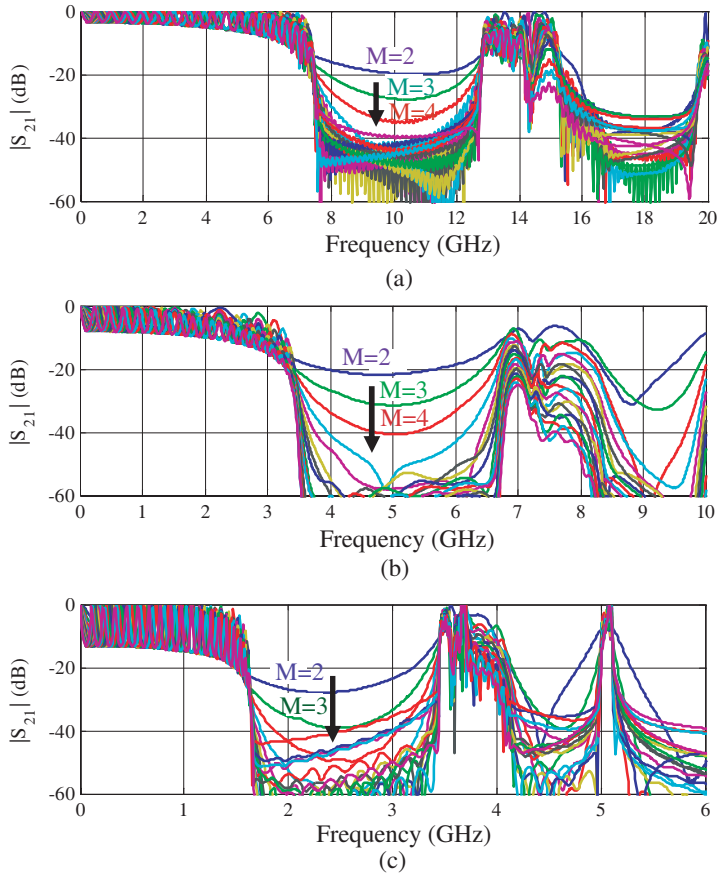

Figure 10. $|S_{21}|$for several $M \times 1$ models, with $M = 2, 3, \ldots, 20$. The f_{Low} increases for larger values of M. (a) Models with patch size $b = 5\,\text{mm}$. (b) Models with patch size $b = 10\,\text{mm}$. (c) Models with patch size $b = 20\,\text{mm}$.

for the three cases ($b = 5$, 10, 20 mm). The f_{Low} becomes constant for $M > 8$, as shown in Figure 11, leading to a minimum error between the predicted value from (9) and the simulated data, as in Figure 12. Although the analytical prediction of f_{Low} is not very accurate, (9) represents an upper bound, thus the real structures will always have a wider band-gap than the one analytically designed.

$$Error\,(\%) = \frac{f_{\text{Low\_}eq.(9)} - f_{\text{Low\_}Sim}}{f_{\text{Low\_}Sim}} \cdot 100 \tag{12}$$

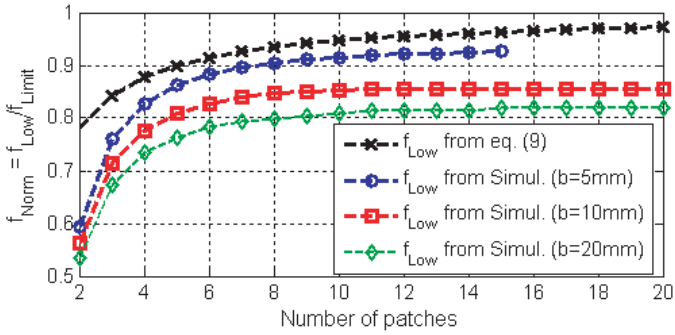

Figure 11. Evaluation of f_{Norm} based on the analytical calculation of f_{Limit} as from the definition in (10); f_{Low} is computed from (9), black-dashed curve, and from the simulated data reported in Figure 10.

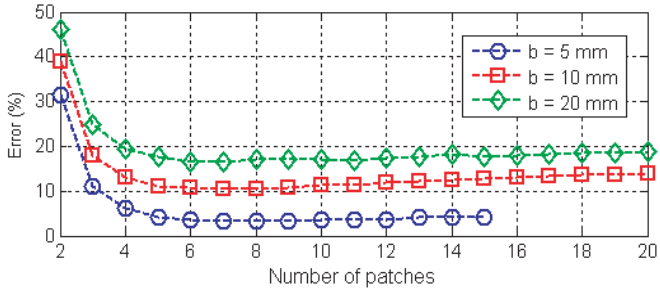

Figure 12. Error evaluation between the f_{Low} from (9) and the f_{Low} extracted from the simulated data in Figure 10.

3.2. $M \times N$ Matrix of Patches

Similar considerations as in Section 3.1 for the $M \times 1$ array can be done for the more general case of a $M \times N$ matrix of patches. The Equations (9)–(10) for the $M \times 1$ case becomes (13)–(14) for the $M \times N$ case.

$$f_{\text{Low}} = f_{TM_{M-1,N-1}} = \frac{c_0}{2\sqrt{\varepsilon_r}} \frac{\mu_0 d}{b}$$

$$\sqrt{\left(\frac{M-1}{M \cdot L_{patch} + (M-1) \cdot L_{bridge}}\right)^2 + \left(\frac{N-1}{N \cdot L_{patch} + (N-1) \cdot L_{bridge}}\right)^2} \quad (13)$$

$$f_{\text{Limit}} \triangleq \lim_{M,N \to \infty} f_{\text{Low}} = \frac{c_0 \mu_0 d}{\sqrt{2} b \sqrt{\varepsilon_r}} \frac{1}{L_{patch} + L_{bridge}} \quad (14)$$

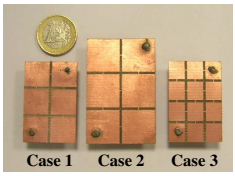

Figure 13. Picture of the three EBG test boards.

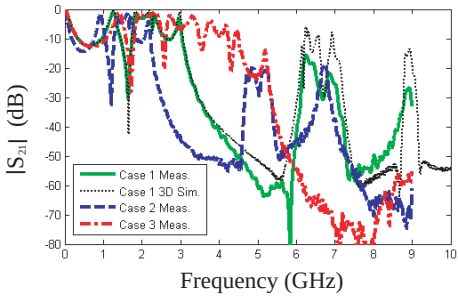

Figure 14. Measured $|S_{21}|$for the three EBG test boards.

The f_{Limit} has been evaluated considering the 10 mm patch size and the other geometry parameters as in the previous section ($w = 0.5\,\text{mm}$, $g = 1\,\text{mm}$, $d = 0.4\,\text{mm}$, $t = 0.017\,\text{mm}$, $\varepsilon_r = 4.4$). The L_{patch} and L_{bridge} values computed as in (6) and (8) are 0.5 nH and 0.39 nH, respectively, as in Section 3.1. These values leads to an $f_{\text{Limit}} = 5.66\,\text{GHz}$, that is $\sqrt{2}$ times greater than the value associated with the $M \times 1$ case ($f_{\text{Limit}} = 4.0\,\text{GHz}$). We can state that a large 2D matrix of patches, although it can be used to fill an entire power plane in multilayer PCB, increases the band-gap f_{Low}. This leads to decrease the band-gap width since the upper limit f_{High} remains unchanged (it is function only of the patch and bridge sizes, not of the patch number).

Similarly for the $M \times 1$ case, the analytical evaluation of the f_{Low} for the $M \times N$ case provides larger values for an increasing number of patches; this is valid both for the x and y directions.

4. EXPERIMENTAL VALIDATION

Three test boards are built to validate the proposed analytical approach. The stack-up geometry is characterized by dielectric thickness $d = 0.508\,\text{mm}$, $\varepsilon_r = 3$, $tg\delta = 0.0015$. The bridge dimensions are maintained constant for the three cases, $g = 1.3\,\text{mm}$, $w = 0.4\,\text{mm}$. The differences among the three models are as follows:

- Case 1: $a = b = 13.7\,\text{mm}$. $M = 3$, $N = 2$.
- Case 2: $a = b = 18\,\text{mm}$. $M = 3$, $N = 2$.
- Case 3: $a = 9.95\,\text{mm}$, $b = 8.7\,\text{mm}$. $M = 4$, $N = 3$.

The pictures in Figure 13 show the three test boards. The solder balls identify the inner pin of the SMA connector that are mounted

Table 1. Band-gap limits f_{Low} and f_{High} extracted from the measured data and computed through the proposed approach. Error evaluation between the two data sets.

Test Case	Data Type	f_{Low} (GHz)	Error on f_{Low}	f_{High} (GHz)	Error on f_{High}
1. 3×2 (a = 13.7 mm)	Analytical	3.35	13.6 %	6.32	1.7 %
	Measured	2.95		6.21	
2. 3×2 (a = 18 mm)	Analytical	2.55	17.5 %	4.8	0.84 %
	Measured	2.17		4.76	
3. 4×3	Analytical	5.56	6.9 %	8.7	4.63 %
	Measured	5.2		8.31	

on the back solid layer. The boards are measured with a 50 MHz-9 GHz VNA (Anritsu MS4624B). The measurement results are given in Figure 14. Case 1 test board is modeled, and the simulation results are included in Figure 14 (dotted line). The curves related to the measured and simulated Case 1 test board agree well to each other. The f_{High} for Case 3 is not very clear since the SMA connector is placed close to the patch center, thus the TM_{10} mode of the single patch cavity is weakly excited; the f_{High} occurs at 8.31 GHz, with an amplitude below −60 dB. The band-gap limits are extracted from the measured data and they are included in Table 1. These results are compared to those computed by applying (3)–(8) for the f_{Low}, and by applying (2) for the f_{High}. The error between the measured and the computed band-gap limits is evaluated as don similarly in (12). The f_{Low} error is consistent to the values shown in Figure 12. Although Figure 12 is related to the $M \times 1$ case, the errors for Case 1 and Case 2 ($M = 3$, $N = 2$) are larger than that for Case 3 ($M = 4$, $N = 3$). The error is larger for Case 2 that has a larger patch (17.5% error, $a = 18$ mm) with respect to Case 1 (13.6% error, $a = 13.7$ mm), as could be expected from the results in Figure 12. The error associated with the analytical evaluation of the f_{High} is very small, below 5 %. The error is proportional to the ratio between the bridge length g and patch size a (b), as stated in Figure 5. It goes from 0.84% for Case 2 ($g/b = 7.2\%$), to 1.7% for Case 1 ($g/b = 9.5\%$), to 4.63 % for Case 3 ($g/b = 13\%$).

5. CASE STUDY

The previous analysis has been applied to a specific case of a 2-layer power bus as part of a multilayer PCB. Typical uses of the EBG are mainly focused on the layout of a complete plane. However other

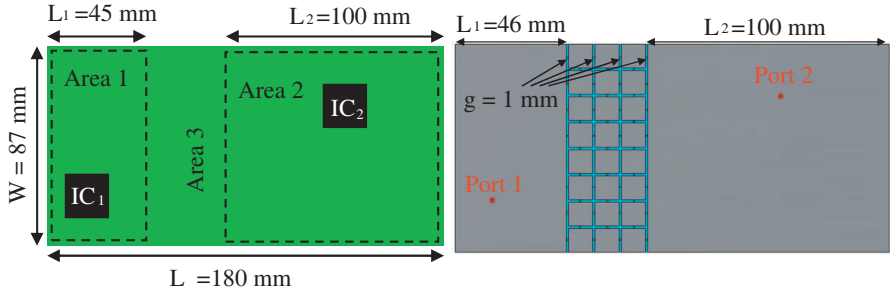

Figure 15. (a) Geometry of the 2-layer PCB considered in the example. (b) Design of the 3×8 EBG to fit the unconstrained Area 3.

layout constrains can limit the EBG design on the entire plane. The example presented herein introduces the possibility to design the EBG only on a limited plane section, to be freely laid out where it is more appropriate without affecting other system functionalities. This application example of the EBG geometry is aimed to isolate two sections of the PCB, Area 1 and Area 2, where two high speed ICs are located, IC_1 and IC_2, as from Figure 15. These ICs generate high speed digital signals at a data rate of 10Gb/s; thus considering the possible noise source related to a band centered at the data rate fundamental harmonic, 5 GHz. The important geometry features of the overall board are shown in Figure 15. The dielectric between the two metal planes is 0.4 mm thick; it has a dielectric permittivity $\varepsilon_r = 4.4$.

The lower GND plane is kept solid, whereas the top plane, PWR, is employed to include an EBG geometry. Limiting the EBG area can avoid problems related to signal integrity (i.e., a solid plane is always preferred as signal reference). Therefore the limited EBG portion can be laid out wherever is more appropriate according to other constrains, i.e., in Area 3 in Figure 15, with the following size: $L_{\mathrm{EBG}} = 35\,\mathrm{mm}$ and $W_{\mathrm{EBG}} = 87\,\mathrm{mm}$.

The size of the EBG analyzed in Section 3 ($a = b = 10\,\mathrm{mm}$, $w = 0.5\,\mathrm{mm}$, $g = 1\,\mathrm{mm}$) can achieve a band-gap centered at about 5 GHz; these dimensions will be considered for designing the EBG for the Area 3. According to the size of Area 3, a 3×8 EBG matrix of patches could fully cover this plane portion, with overall size 34 mm by 87 mm. In the case of Area 1 and Area 2 having associated the same voltage level, the DC connection between the two areas could be preferable; thus the EBG section can be designed to be connected to the two areas through bridges with the same size as the EBG bridges. Beside the large 3×8 configuration, a second EBG geometry is designed with 1×8 array of patches, keeping just the second row of

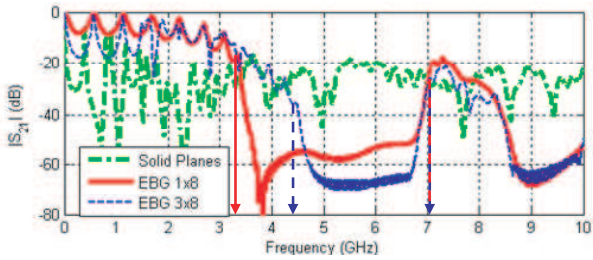

Figure 16. $|S_{21}|$ for the geometry made by two solid planes, the 1×8 and the 3×8 EBG structures.

the 3×8 configuration. This second model leads to make the Area 1 and Area 2 larger, with $L_1 = 57\,\text{mm}$ and $L_2 = 111\,\text{mm}$. The two EBG geometries are first simulated separately, similarly to the simulation models shown in Section 3. The simulation results are shown in Figure 16 together with the $|S_{21}|$ of the solid plane geometry. The prediction of the band-gap f_{Low} by the proposed analytical procedure provides $f_{\text{Low}} = 3.7\,\text{GHz}$ and $f_{\text{Low}} = 4.85\,\text{GHz}$ for the case 1×8 and 3×8 EBG, respectively. These results agree well to the last visible resonant mode before the band-gap (3.34 GHz and 4.46 GHz, respectively) identified in the solid and dashed curves in Figure 16. Also the f_{High} from the 3D simulation (7.06 GHz) is correctly predicted by (2), 7.15 GHz. The simulation ports in the large plane model are placed at the locations of IC_1 and IC_2. Although the two EBG structures have different band-gap lower limits, they both include a band around 5 GHz. The 1×8 structure provides a more robust design with a band-gap going from 3.34 GHz to 7.06 GHz. The 3×8 geometry, instead, with a $f_{\text{Low}} = 4.46\,\text{GHz}$, has a band-gap not centered around 5 GHz; however it is more effective providing larger noise reduction. The two EBG configurations are included in the full model, as in Figure 15(b) for the 3×8 case.

The EBG geometry designed as proposed in Figure 15 achieves a sort of fence isolating the two areas, keeping, below the band-gap, a similar behavior as the solid plane case. This can be seen in the simulation results in Figure 17 and in the $|Z_{11}|$ curve plotted in Figure 18. The small shift, in the $|Z_{11}|$ toward lower frequencies of the first resonant mode, from 400 MHz to 360 MHz, and to 320 MHz, for the 1×8 and the 3×8 case, respectively, can be managed by accordingly selecting and placing decoupling capacitors. The better isolation between the two areas is obtained with the implementation of the 3×8 EBG geometry that achieve the largest reduction in the $S|_{21}|$ from around 4 GHz to 7 GHz. This 3×8 EBG provides about

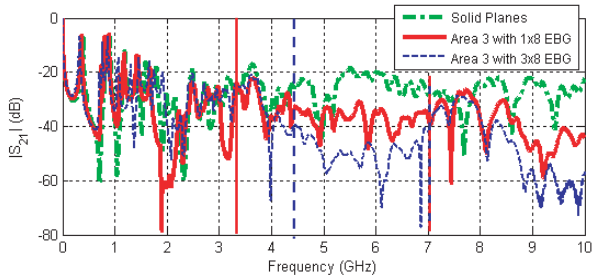

Figure 17. $|S_{21}|$ for the geometry made by two solid planes, and the planes after including the 1×8 or the 3×8 EBG structures between Area 1 and Area 2.

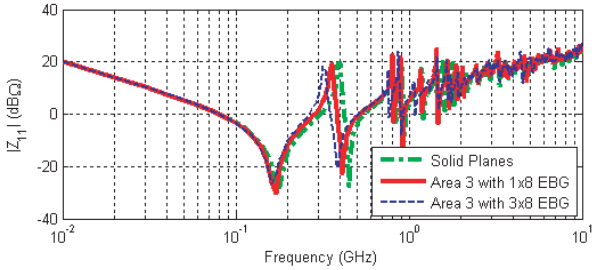

Figure 18. $|Z_{11}|$for the geometry made by two solid planes, and the planes after including the 1×8 and the 3×8 EBG structures.

10 to 20 dB of noise reduction with respect to the original solid plane case, and 5 to 10 dB with respect to the 1×8 EBG case. Thus the EBG with three rows (3×8) is more effective than the 1×8 EBG case, if no constrains on layout space force to use the 1×8 EBG.

6. CONCLUSIONS

The present paper introduces a complete procedure for the analysis of planar electromagnetic band-gap structures based on the concept of total inductance. A patterned EBG plane together with a solid plane underneath generates a cavity that has associated more inductance than the ideal cavity counterpart made by two solid planes. This procedure allows a quick and accurate evaluation of the band-gap lower limit f_{Low}. The study also provides a more precise evaluation of the band-gap upper limit f_{High} quantifying the effect of the parameters altering its analytical calculation. The value of the f_{Low} is studied as a function of the number of patches, finding out that it reaches

an asymptotic value when the number of patches goes toward infinity, while keeping constant the geometrical and electrical properties of the structure. This limit allows a quick evaluation of the f_{Low}. Then the analytical expression of the f_{Low} gives a more precise calculation taking into account the number of patches chosen according to the available layout area. The $M \times 1$ array achieves a lower f_{Low} rather then the $M \times N$ case, thus a wider band-gap due to the constant f_{High}. The $M \times N$ configuration, instead, could be more helpful when using the EBG for a partial filling of the plane, achieving better noise isolation along both directions, as demonstrated in the practical example. The layout option of partial EBG has been shown to be effective for noise coupling reduction between two PCB areas, without the need of patterning the whole plane, thus keeping the ideal solid reference where required by other constrains.

REFERENCES

1. Berghe, S. V., F. Olyslager, D. de Zutter, J. D. Moerloose, and W. Temmerman, "Study of the ground bounce caused by power plane resonances," *IEEE Trans. Electromagn. Compat.*, Vol. 40, No. 2, 111–119, May 1998.
2. Na, N., J. Jinseong, S. Chun, M. Swaminathan, and J. Srinivasan, "Modeling and transient simulation of planes in electronic packages," *IEEE Trans. Adv. Packag.*, Vol. 23, No. 3, 340–352, Aug. 2000.
3. Lei, G. T., R. W. Techentin, P. R. Hayes, D. J. Schwab, and B. K. Gilbert, "Wave model solution to the ground/power plane noise problem," *IEEE Trans. Instrum. Meas.*, Vol. 44, No. 2, 300–303, Apr. 1995.
4. Okoshi, T., *Planar Circuits for Microwaves and Lightwaves*, Ch. 3, Springer-Verlag, Berlin, Germany, 1985.
5. Oo, Z. Z., E. X. Liu, E. P. Li, X. Wei, Y. Zhang, M. Tan, L. W. J. Li, and R. Vahldieck, "A semi-analytical approach for system-level electrical modeling of electronic packages with large number of vias," *IEEE Trans. Adv. Packag.*, Vol. 31, No. 2, 267–274, May 2008.
6. Huang, W.-T., C.-H. Lu, and D.-B. Lin, "The optimal number and location of grounded vias to reduce crosstalk," *Progress In Electromagnetics Research*, Vol. 95, 241–266, 2009.
7. Wu, B. and L. Tsang, "Full-wave modeling of multiple vias using differential signaling and shared antipad in multilayered

high speed vertical interconnects," *Progress In Electromagnetics Research*, Vol. 97, 129–139, 2009.

8. Choi, J., V. Govind, R. Mandrekar, S. Janagama, and M. Swaminathan, "Noise reduction and design methodology for the mixed-signal systems with alternating impedance electromagnetic bandgap (Al-EBG) structure," *IEEE MTT-S Int. Microw. Symp. Dig.*, 645–651, Long Beach, CA, Jun. 2005.
9. Kim, T. H., D. Chung, E. Engin, W. Yun, Y. Toyota, and M. Swaminathan, "A novel synthesis method for designing electromagnetic bandgap (EBG) structures in packaged mixed signal systems," *Proc. 56th Electron. Compon. Technol. Conf.*, 1645–1651, 2006.
10. Sievenpiper, D., L. Zhang, R. F. J. Broas, N. G. Alexopolous, and E. Yablonovitch, "High impedance electromagnetic surfaces with a forbidden frequency band," *IEEE Trans. Microw. Theory Tech.*, Vol. 47, No. 11, 2059–2074, Nov. 1999.
11. Moghadasi, S. M., A. R. Attari, and M. M. Mirsalehi, "Compact and wideband 1-d mushroom-like EBG filters," *Progress In Electromagnetics Research*, Vol. 83, 323–333, 2008.
12. Kim, S.-H., T. T. Nguyen, and J.-H. Jang, "Reflection characteristics of 1-D EBG ground plane and its application to a planar dipole antenna," *Progress In Electromagnetics Research*, Vol. 120, 51–66, 2011.
13. Hajj, M., R. Chantalat, M. Lalande, and B. Jecko, "Sectoral M-EBG antenna with multipolarization capabilities for wimax base stations," *Progress In Electromagnetics Research C*, Vol. 22, 211–229, 2011.
14. Khromova, I., I. Ederra, R. Gonzalo, and B. P. de Hon, "Symmetrical pyramidal horn antennas based on EBG structures," *Progress In Electromagnetics Research B*, Vol. 29, 1–22, 2011.
15. Xie, H.-H., Y.-C. Jiao, L.-N. Chen, and F.-S. Zhang, "An effective analysis method for EBG reducing patch antenna coupling," *Progress In Electromagnetics Research Letters*, Vol. 21, 187–193, 2011.
16. Hubing, T. H., J. L. Drewniak, T. P. Van Doren, and D. M. Hockanson, "Power-bus decoupling on multi-layer printed circuit boards," *IEEE Trans. Electromagn. Compat.*, Vol. 37, 155–166, May 1995.
17. Eom. D.-S., J. Byun, and H.-Y. Lee, "New composite power plane using spiral ebg and external magnetic material for SSN suppression," *Progress In Electromagnetics Research Letters*, Vol. 15, 69–77, 2010.

18. He, H.-S., X.-Q. Lai, Q. Ye, Q. Wang, W.-D. Xu, J.-G. Jiang, and M.-X. Zang, "Wideband SSN suppression in high-speed PCB using novel planar EBG," *Progress In Electromagnetics Research Letters*, Vol. 18, 29–39, 2010.
19. Tavallaee, A. and R. Abhari, "2-D characterization of electromagnetic bandgap structures employed in power distribution networks," *IET Microw. Antennas Propag.*, Vol. 1, 204–211, Feb. 2007.
20. Kamgaing, T. and O. M. Ramahi, "Design and modeling of high impedance electromagnetic surfaces for switching noise suppression in power planes," *IEEE Trans. Electromagn. Compat.*, Vol. 47, No. 3, 479–489, Aug. 2005.
21. Wang, T.-K., T. W. Han, and T.-L. Wu, "A novel power/ground layer using artificial substrate EBG for simultaneously switching noise suppression," *IEEE Trans. Microw. Theory Tech.*, Vol. 56, No. 5, 1164–1171, May 2008.
22. Wu, T.-L., H.-H. Chuang, and T.-K. Wang "Overview of power integrity solutions on package and PCB: Decoupling and EBG isolation," *IEEE Trans. Electromagn. Compat.*, Vol. 52, No. 2, 346–356, May 2010.
23. Wu, T. L., Y. H. Lin, T. K. Wang, C. C. Wang, and S. T. Chen, "Electromagnetic bandgap power/ground planes for wideband suppression of ground bounce noise and radiated emission in high-speed circuits," *IEEE Trans. Microw. Theory Tech.*, Vol. 53, No. 9, 2935–2942, Sep. 2005.
24. Mohajer-Iravani, B., S. Shahparnia, and O. M. Ramahi, "Coupling reduction in enclosures and cavities using electromagnetic band gap structures," *IEEE Trans. Electromagn. Compat.*, Vol. 48, No. 2, 292–303, May 2006.
25. De Paulis, F., L. Raimondo, S. Connor, B. Archambeault, and A. Orlandi, "Design of a common mode filter by using planar electromagnetic band-gap structures," *IEEE Trans. on Advanced Packaging*, Vol. 33, No. 4, 994–1002, Nov. 2010.
26. De Paulis, F., L. Raimondo, S. Connor, B. Archambeault, and A. Orlandi, "Compact configuration of a planar EBG based CM filter and crosstalk analysis," *IEEE International Symposium on EMC*, Long Beach, CA, USA, Aug. 14–19, 2011.
27. Mohajer-Iravani, B. and O. M. Ramahi, "Wideband circuit model for planar EBG structures," *IEEE Trans. Adv. Packag.*, Vol. 33, No. 2, 345–354, May 2010.
28. Toyota, Y., E. Engin, T. Kim, M. Swaminathan, and K. Uriu, "Stopband prediction with dispersion diagram for electromagnetic

bandgap structures in printed circuit boards," *Proc. IEEE EMC Symp.*, 807–811, Portland, OR, Aug. 2006.

29. Kim, K. H. and J. E. Schutt-Aine, "Analysis and modeling of hybrid planartype electromagnetic-bandgap structures and feasibility study on power distribution network applications," *IEEE Trans. Microw. Theory Tech.*, Vol. 56, No. 1, 178–186, Jan. 2008.
30. Kim, T. H., D. Chung, E. Engin, W. Yun, Y. Toyota, and M. Swaminathan, "A novel synthesis method for designing electromagnetic band gap (EBG) structures in packaged mixed signal systems," *Proc. 56th Electron. Compon. Technol. Conf.*, 1645–1651, San Diego, CA, May 30–Jun. 2, 2006.
31. Raimondo, L., F. De Paulis, and A. Orlandi, "A simple and efficient design procedure for planar electromagnetic bandgap structures on printed circuit boards," *IEEE Transaction on Electromagn. Compat.*, Vol. 53, No. 2, 482–490, May 2010.
32. Pozar, D. M., *Microwave Engineering*, 3rd Edition, Wiley, New York, 2005.
33. Computer Simulation Technology, *CST Studio Suite*, 2011, Available: http://www.cst.com/.